Microscopic versus macroscopic diffusion in model membranes by Electron Spin Resonance spectral-spatial imaging

Y.-K. Shin, U. Ewert, D. E. Budil, and J. H. Freed
Baker Laboratory of Chemistry, Cornell University, Ithaca, New York 14853 USA

ABSTRACT The macroscopic and the microscopic diffusion coefficients of a phospholipid spin label (16-PC) in the model membrane 1-palmitoyl-2-oleoyl-*sn*-glycero-phosphatidylcholine have been measured simultaneously in the same sample utilizing the new technique of spectral-spatial electron spin resonance imaging. The macroscopic diffusion coefficient D_{macro} for self-diffusion of 16-PC spin label is obtained from imaging the concentration profiles as a function of time, and it is $(2.3 \pm 0.4) \times 10^{-8}$ cm^2/s at 22°C. The microscopic diffusion coefficient D_{micro} for relative diffusion of the spin probes is obtained from the variation of the spectral line broadening with spin label concentration, which is due to spin–spin interactions. D_{micro} is found to be substantially greater than D_{macro} for the same sample at the same conditions, and is estimated to be at least $(1.0 \pm 0.4) \times 10^{-7}$ cm^2/s. Possible sources for their difference are briefly discussed in terms of the models used for D_{micro}.

INTRODUCTION

Lateral diffusion of membrane components is a fundamental property of fluid biomembranes. Translational diffusion of lipids and proteins is essential for various biological processes (1). A variety of techniques have been developed to measure the translational diffusion coefficients in model or biomembranes. The techniques can be divided into two general categories according to the distance scale of measurement. Macroscopic methods, such as NMR-spin echo (2, 3), fluorescence recovery after photobleaching (FRAP) (4, 5), and dynamic imaging of diffusion by electron spin resonance (ESR) (6–9) measure changes in the bulk distribution of labeled molecules with time, and generally cover distances of a few to a few hundred micrometers. Microscopic methods measure diffusion over lengths of the order of molecular diameters, i.e., a few tens of angstroms. Such techniques detect encounters between labeled molecules by excimer formation (10), quasielastic neutron scattering (11), or Heisenberg spin exchange (HE) (12–17).

Macroscopic experiments are, in general, interpreted in terms of simple phenomenological descriptions of diffusion (e.g., Fick's second law) to yield the self-diffusion coefficient. However, for microscopic methods, the analysis leading to the relative diffusion coefficient depends heavily upon the choice of the microscopic molecular dynamic model, resulting in considerable uncertainty in the estimated diffusion coefficient. Furthermore, since such methods detect encounters between labeled molecules, the nature of the mixing of the label molecule in the fluid will be a relevant factor. Nevertheless, these methods are extremely important for investigating the microscopic dynamic molecular structure of membranes. In many cases, the model-independent macroscopic diffusion coefficient can provide a "benchmark" for interpreting experiments on microscopic molecular transport processes. An ideal experiment for such a comparison would be one in which the macroscopic and the microscopic diffusion coefficients are simultaneously measured in the same sample.

Dynamic imaging of diffusion by ESR (DID-ESR) has been very successful in accurately measuring the macroscopic diffusion coefficients of spin labels in model membranes (7, 8). However, this method requires that the ESR spectrum be independent of position throughout the sample. Therefore, the spin label concentration must be kept low enough to ensure that any changes in ESR line shape due to spin–spin interactions are negligible.

Spectral-spatial ESR imaging (18–21) is a promising new technique for generalizing DID-ESR to study diffusion of spin probes in systems with substantial spin concentration. Spectral-spatial ESR imaging provides a way to resolve the concentration (or position) dependent spectral variation in a two-dimensional fashion as illustrated in Fig. 1: i.e., along one axis (the spatial axis) it gives the spin concentration profile, whereas along the other axis it gives the ESR spectrum at that position (and spin concentration). This method has previously been illustrated for the investigation of transport in

Dr. Ewert is on leave from the Center of Scientific Instruments, Academy of Sciences, G.D.R.

0006-3495/91/04/950/08 $2.00

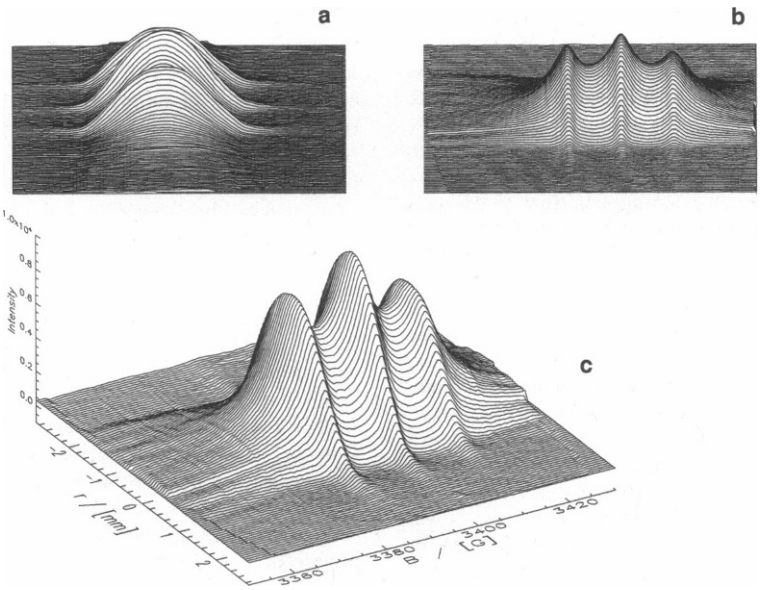

FIGURE 1 ESR Spectral-spatial image of the 16-PC nitroxide spin probe diffusing in aligned multilayers of the lipid POPC viewed (*a*) along the spectral axis to display the spatial distribution, (*b*) along the spatial axis to display the spectral dependence on position, and (*c*) in perspective.

nonuniform media (22) and for studying O_2 distributions (23).

In this report we present our successful simultaneous measurement of both the macroscopic and microscopic diffusion coefficients, D_{macro} and D_{micro}, respectively, of a spin-labeled phospholipid in a model membrane utilizing a substantial spin concentration and spectral-spatial ESR imaging. If the spin probe is initially concentrated in a small region of the sample, its distribution will tend over time to become homogeneous via translational diffusion. By measuring several spectral-spatial images at different times, we can analyze the spread of the concentration profile as a function of time to obtain the macroscopic diffusion coefficient from the diffusion equation, by analogy with the DID-ESR method (7, 24).

In addition, the macroscopic diffusion will produce a continuous variation of spin concentration along the spatial axis. Thus, at a later time one can obtain an entire set of concentration-dependent ESR spectra from the spectral-spatial image of just a single sample. Such an experiment will be equivalent to the spectra obtained from many different homogeneous samples that must be prepared with different spin concentrations for conventional ESR studies of HE (17, 14, 16). The ESR line broadening that results from spin relaxation induced by spin–spin interactions such as HE can be analyzed to obtain the microscopic diffusion coefficient.

Devaux and McConnell (25) years ago (before the development of ESR imaging) used the concentration dependence of the ESR spectrum together with an inhomogeneous initial distribution of spin labeled lipids to measure D_{macro}. The spatial distribution was deduced by a complicated simulation of the composite spectrum as a superposition of spectra from regions of different concentration, which also required many reference spectra. Spectral-spatial imaging effectively separates the spectra for each concentration, permitting a direct determination of D_{macro} as well as D_{micro} from the line broadening.

In comparing the results on macroscopic diffusion via ESR imaging vs. microscopic diffusion via spin–spin interactions, it is important to note that the former provides the macroscopic tracer diffusion coefficient of the spin label, which can be identified as the self-diffusion coefficient of the lipid in cases when the two are very similar (7, 8); however, the latter provides a microscopic *relative* diffusion coefficient which has been shown to be very sensitive, not only to diffusion, but also to relative interactions between colliding spin labels, and how they are influenced by their milieu (17, 26). Clearly also the probability of biomolecular collisions is influenced by any nonideal mixing of the spin labels (17, 26).

MATERIALS AND METHODS

Materials and sample preparation

1-Palmitoyl-2-oleoyl-*sn*-glycero-phosphatidylcholine (POPC) was purchased from Avanti Polar Lipids Inc. (Birmingham, AL) and was used

without further purification. The 1-palmitoyl-2-(16-doxyl stearoyl)phosphatidylcholine (16-PC) was a gift from Professor G. W. Feigenson (Dept. of Biochemistry, Cornell University). The purity of 16-PC was tested by thin layer chromatography, and it was found to contain $< 2\%$ impurity.

Utilizing our well-developed techniques for preparing samples with an initial inhomogeneous distribution of labeled lipids (6–8), a well-aligned POPC multilayer sample having a narrow (~ 0.5 mm) strip of POPC/16-PC mixture in the middle was prepared. The initial spin probe concentration in the narrow strip was 9.1 ± 0.3 mol %. Water content in the sample was $\sim 20\%$ by weight.

The total number of spins in the sample could be determined from the initial spatial distribution of spin label obtained by ESR imaging (*vide infra*) shortly after its preparation. This initial distribution showed a plateau with rounded edges and a flat region of ~ 0.3 mm width corresponding to the 9.1 mol % strip of spin-labeled lipid, which is used to calibrate the initial mole fraction distribution, $x_0(z)$. An integration of this initial spatial distribution will give the total number of spins, $n = \int x_0(z)dz\,[d_M\, hl]$, where d_M is the molar density, and h and l are the height and length of the sample. At later times, $x(z, t)$ will change, but the integral $\int x(z, t)dz = n/d_M hl$ remains independent of time. This fact was used to calibrate the $x(z, t)$ for later times. We estimate an error of no more than 5% in this integral, which is mainly due to baseline correction of the reconstructed image.

Spectral-spatial Imaging

The basic premise underlying spectral spatial imaging methods is that the spatial dependence of the ESR spectral intensity can be represented as a "pseudo-object" in a space consisting of an intrinsic frequency coordinate (the spectral dimension) and one or more spatial dimensions. Fig. 1 shows an example of such an object in one spectral and one spatial dimension. The imaging method used is the multiple stepped gradient (18–21) (in earlier papers [27, 28] called the "graduated field gradient") algorithm. In this technique, one sweeps through the ESR spectrum repeatedly, each time with a different constant linear magnetic field gradient. The effect of the gradient is to cause the ESR spectrum at each spatial coordinate to shift relative to the spectral axis by an amount that depends upon its spatial location. The signal recorded during a spectrometer field sweep measures the superposition of spectra from all points in the spatial dimension, i.e., the convolution of the spectral and spatial distributions. This is equivalent to measuring the projection of the pseudo-object after it is rotated through some angle α, given by

$$G(\alpha) = \frac{\Delta S}{\Delta R} \cdot \cot \alpha, \tag{1}$$

where $G(\alpha)$ is the field gradient, ΔS is the spectral width, and ΔR is the size of the object. Once projections are collected for a set of rotation angles, α, the image of the spectral-spatial object can be reconstructed using standard tomographic methods. Angles near 0 and π are unavailable due to the finite limitation on the field gradient (cf. Eq. 1); however, these projections may be interpolated using a modified iterative limited angle algorithm described by Maltempo et al. (21). Details of these methods have been discussed in references 18–21, 29, and 30.

Our experiments were performed on an ER200D-SRC spectrometer (Bruker Instruments, Inc., Billerica, MA) with an E30 magnet. The gradient was varied using a ZZG1 imaging device constructed at the Center of Scientific Instruments of the Academy of Sciences of the G.D.R. The imaging device consists of two bidirectional 400 VA power amplifiers and two water-cooled gradient coils mounted on a TE_{102} cavity. The cavity coil unit is centered with a differential screw set in the magnet, and the coils produce a linear field gradient along the homogeneous magnetic field direction, z. The experiment was controlled by an EPS-286 (IBM-AT compatible) computer equipped with a DT2821 board (Data Translation, Inc., Marlborough, MA) for data acquisition and for setting the field gradients and scan trigger. The computer is interfaced to the spectrometer's IEEE-488 bus using a National Instruments GPIB-PC/IIA board to adjust the spectrometer time constant, modulation amplitude, receiver gain, and field offset. Scan range, time constant, and modulation amplitude were set proportional to $(\sin \alpha)^{-1}$ for each scan. Further details of the experimental apparatus and methods will be presented elsewhere (U. Ewert and J. H. Freed, manuscript in preparation).

The imaging device and data acquisition software were optimized for a 128×128 data matrix containing a circle in which the final image was reconstructed. For this matrix dimension, the maximum field gradient of 395 G/cm provided a spatial resolution of 100 μm and a spectral resolution of 0.6 G (scaled to the half width at half height of Gaussian lines). To increase the spatial resolution we used a projection reconstruction algorithm with a spatial "zoom" of two; that is, the reconstruction matrix was subdivided into 256 spatial and 128 spectral data points and only the inner 128 spatial points were stored. Each projection was measured with 256 samples, and the modulation amplitude and time constant were selected appropriately for the smallest linewidth. This procedure provided an intrinsic spatial resolution of 50 μm. The enlarged limited angle and resulting nonlinear stepping in α required highly accurate limited-angle interpolations to avoid artifacts. A total of 91 projections were measured for $7.2° \leq \alpha \leq 172.8°$ using a constant magnetic field scan speed of 73 G/s. The total time for the measurement was 7 min, of which one minute was used for remote control, computer tasks, field recovery, and field prescan. After the limited angle interpolations, a nonlinear least squares fit was used to parameterize the image. The spectrum at each position was fit to a set of three Lorentzian lines, and the image was integrated across the spectral dimension and fit to a Gaussian distribution in the spatial dimension. The *effective* spectral and spatial resolutions as estimated from the uncertainties in the fit of the linewidths of the Lorentzians and the width of the Gaussian distribution are 0.08 G and 10 μm, respectively.

RESULTS AND ANALYSIS

The macroscopic diffusion coefficient D_{macro} is determined utilizing Fick's second law for diffusion (24):

$$\frac{\partial C(x, t)}{\partial t} = D_{macro} \frac{\partial^2 C(x, t)}{\partial x^2}. \tag{2}$$

Integration of the spectral-spatial image intensity along the spectral axis in Fig. 1 gives the spatial profile of the spin concentration at a given time. Immediately after sample preparation, the initial spatial profile appears as a narrow plateau with rounded edges. After the samples are allowed to diffuse for ~ 2 h at room temperature, the concentration profile is well approximated by a Gaussian distribution (see Fig. 1), and its time-dependence, $C(x, t)$ is given by

$$C(x, t) = \frac{C_0}{\sqrt{2\pi \cdot \sigma^2(t)}} \exp\left(-\frac{x^2}{2\sigma^2(t)}\right), \tag{3}$$

where the variance $\sigma^2(t) = \delta^2(0) + 2D_{macro}t$ and $\delta^2(0)$ is the variance of a Gaussian profile at $t = 0$ (9). The plot of $\sigma^2(t)$ vs. t is shown in Fig. 2; the time needed for the macroscopic diffusion measurement was ~10 h, which corresponds to an average molecular displacement $\Delta r = \sqrt{2Dt} \sim 400$ μm. D_{macro} determined from the slope in Fig. 2 is $(2.3 \pm 0.4) \times 10^{-8}$ cm²/s at 22°C, which agrees rather well with our previous result on the same system ($D_{macro} \sim 3 \times 10^{-8}$ cm²/s) (7) and the FRAP result of Vaz et al. ($D_{macro} \sim 3.5 \times 10^{-8}$ cm²/s for NBD-PE in POPC at 20°C) (5).

A thorough discussion of the analysis of concentration-dependent line broadening has been given elsewhere (17). In summary, the concentration-dependent ESR line broadening can be considered to arise from HE and from electron–electron dipolar (EED) interactions between the electron spins on neighboring spin probe molecules. According to modern HE theory (17, 32, 33), the Heisenberg spin exchange contribution to the line width in the strong exchange limit of exchange broadening, and assuming Brownian diffusion, is given for ^{14}N nitroxides by (12, 17)

$$T_2^{-1}(\text{HE}) = \left(\frac{8\pi}{3}\right) d D_{micro} N_A C f^*, \tag{4}$$

where d is the encounter distance for two spins, D_{micro} is the microscopic self-diffusion coefficient, N_A is the Avogadro number, C is the molar concentration of spins, and f^* is a partition function given by

$$(f^*)^{-1} = d \int_d^\infty \frac{\exp[U(r)/kT]}{r^2}\, dr, \tag{5}$$

in which $U(r)$ is a mean-field pair interaction potential for the spin probe molecules (i.e., the potential of the mean force). In contrast, the EED contributions to the linewidth are (12, 34)

$$T_2^{-1}(\text{EED}) \simeq \hbar^2 \gamma_e^4 \left(\frac{19\pi}{405}\right) \cdot \frac{N_A C}{d D_{micro}} \cdot \{f^* \exp[U(d)/kT]\}^{-1}. \tag{6}$$

Eqs. 4 and 6 express the fact that the linewidth contributions from both HE and EED are expected to be linear with concentration in the limit of ideal solutions. Linearity with concentration is not always observed (17, 26) and it has been suggested that more generally the concentration C should be replaced by the thermodynamic activity of the spin label, especially at higher concentrations (26). To investigate line broadening due to HE and EED, we fit the ESR spectral intensity $I(\omega, x)$ at each spatial location with a sum of three Lorentzian lines corresponding to the ^{14}N nitroxide nuclear spin quantum numbers $M = 1, 0, -1$:

$$I(\omega, x) = R \sum_M \frac{A_M}{A_M^2 + (\omega - \omega_M)^2}, \tag{7}$$

where A_M is the linewidth $(T_2[M]\gamma_e)^{-1}$, ω_M is the resonant frequency for each ESR line, and R is a constant proportional to the spin concentration. The central ESR line ($M = 0$) was used for the present analysis. The spin label concentration in units of mole fraction was obtained as a function of spatial coordinate, as described above. Mole fraction was then converted to an *effective* molar concentration C within the bilayer using the volume V_l of one lipid molecule multiplied by Avogadro's number to give volume per mole: $C = 2x \cdot (V_l N_A)^{-1}$. For the present analysis, V_l was computed as the product of the average area per phospholipid on the membrane surface, $A_l = 75$ Å² and one half the bilayer thickness, $d_l = 17.5$ Å (35). Following Sachse et al. (16) an additional factor of 2 has been introduced into the expression for effective concentration to account for collisions between spin labels on different sides of the bilayer, since the nitroxide moiety is attached close to the end of one of the 16-PC acyl chains. (This factor would be inappropriate for lipids labeled closer to the headgroup, such as 5-PC, and may also be affected by bending of the lipid chains toward the membrane surface, as we discuss below).

Fig. 3 shows a plot of linewidth $\Delta H = (2/\sqrt{3})A_M$ vs. effective concentration derived in this manner. These data show two distinct ranges of spin label concentrations which appear to have different dependences of linewidth on concentration, with a presumed inflection near $x \sim 0.02$. The lower concentration regime is affected by inhomogeneous broadening due to proton superhyperfine structure, which however has been exchanged out in the higher concentration regime (16, 36).

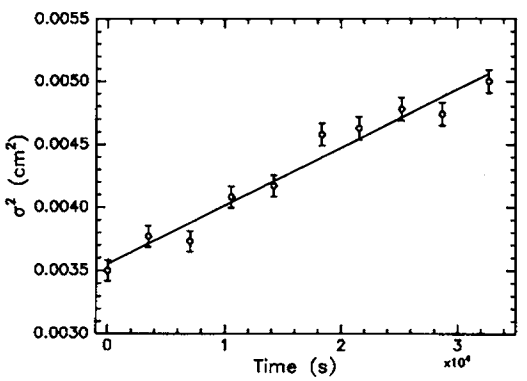

FIGURE 2 Determination of D_{macro} of 16-PC in the POPC bilayer at 22°C by a linear fit of the distribution width, $\sigma^2(t)$, with respect to time.

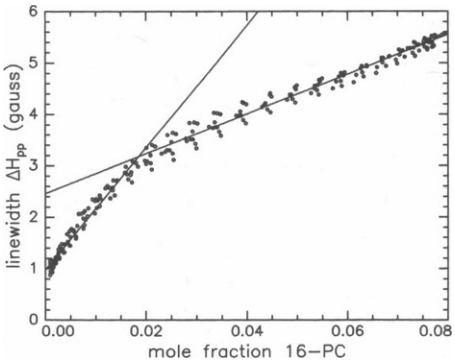

FIGURE 3 Linewidth of central ESR line as a function of mole fraction 16-PC in aligned multilayers of POPC at 22°C. Separate lines were fit to the low ($x < 0.02$) and high ($x > 0.02$) concentration regions as shown.

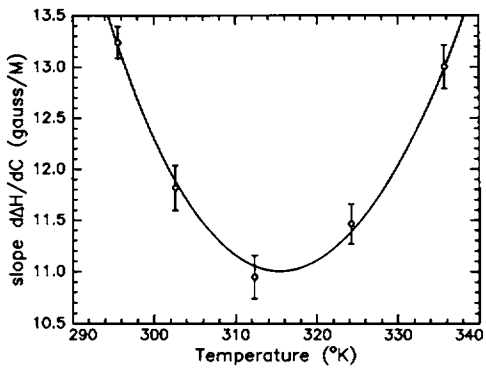

FIGURE 4 Slope $d\Delta H/dC$ as a function of temperature for the higher range of 16-PC mole fraction in POPC. Curve represents the best fit of Eq. 8 with the parameters given in the text.

Given the lineshape distortions due to this source for $x \leq 0.02$ (consistent with the observations of Sachse et al.) as well as the reduced signal-to-noise at these concentrations, we will only treat in detail the results for $x > 0.02$, where the lineshapes are simple Lorentzians.

We investigated the temperature dependence of the slope $d\Delta H/dC$ for the region of high spin probe concentration. Assuming Arrhenius behavior for D_{micro} (i.e., $D_{micro} = D^\circ \exp[-E_{act}/kT]$), the expected temperature dependence of the concentration-dependent linewidth is given by

$$\frac{d\Delta H}{dC} \equiv \left(\frac{2}{\sqrt{3}\gamma_e}\right) \cdot \frac{d[T_2^{-1}(\mathrm{HE}) + T_2^{-1}(\mathrm{EED})]}{\mathrm{dC}}$$
$$= A \exp(-E_{act}/kT)$$
$$+ B[\exp[-U(d)/kT]] \exp(E_{act}/kT), \quad (8)$$

where $A = 3.31 \times 10^{14}$ (dD°) G · l/mol and $B = 1.24 \times 10^{-12}$ $(1/dD^\circ)$ G · l/mol assuming $f^* \approx 1$ (17). The values of $d\Delta H/dC$ at several temperatures were fit to Eq. 8 to yield the three unknown parameters, as shown in Fig. 4. The best fitting parameters are $dD^\circ = (7.9 \pm 2.2) \times 10^{-10}$ cm³/s, $E_{act} = (6.8 \pm 0.4)$ kcal/mol, and $U(d) = (1.6 \pm 0.1)$ kcal/mol in the spin concentration range $0.02 < x < 0.08$. The result for E_{act} compares favorably with the values of $E_{act} = 6.3$ kcal/mol from D_{macro} measured for this sytem by DID-ESR (7).

Eqs. 4 and 6 have been derived for isotropic diffusion in three dimensions. For anisotropic fluids such as membranes, it has been suggested (17, 37) that D in these equations be replaced by the mean of $D_\parallel$, which corresponds to diffusion across the bilayers, and $D_\perp$, which represents lateral diffusion within the plane of the bilayers (i.e., $D \simeq D_{mean} = [D_\parallel + 2D_\perp]/3$). In the case of PC model membranes, we have $D_\perp \gg D_\parallel$, so that $D_{mean} \cong 2/3D_\perp$, and we identify D_{micro} with $D_\perp$. This is a very simple way to introduce lateral motion in a plane as a limiting case of anisotropic three-dimensional motion (cf. the definitions $D \equiv \langle r^2 \rangle/6t$ for three dimensions, vs. $D \equiv \langle r^2 \rangle/4t$ for two dimensions), but see below.

At 22°C we obtain $D_{\perp,micro} = (1.0 \pm 0.4) \times 10^{-7}$ cm²/s when we use a diameter d corresponding to a hard cylinder with cross-sectional area A_l, i.e., $d = 2\sqrt{A_l/\pi} \approx 10$ Å. This value is approximately a factor of four greater than D_{macro}. In comparison, linewidth studies by Sachse et al. (16) yielded $D_{micro} \sim 1.2 \times 10^{-7}$ cm²/s (from the HE contribution) and $D_{micro} \sim 2.6 \times 10^{-7}$ cm²/s (from the EED contribution) at 30°C for 16-PC in a dimiristoyl-*sn*-glycero-phosphatidylcholine (DMPC) model membrane, which compares favorably with our results on POPC. (These authors used a simpler theoretical model which did not correct for $U[d]$ in Eq. 6.)

DISCUSSION

Our measurements of D_{macro} and D_{micro} are in agreement with previous observations that D measured by microscopic techniques is larger than D measured by macroscopic techniques, although the reported discrepancy has been somewhat less than the present results indicate (2, 11). Sackmann et al. (11) have shown that D_{micro} measured by quasielastic neutron scattering is about a factor of 2 larger than D_{macro} measured by FRAP in DPPC model membranes.

At present, the reason for the large discrepancy between D_{micro} and D_{macro} is not clear. Saxton has postulated that such discrepancies could be due to different sample preparation techniques that produce inhomoge-

neous defects in the model membrane (38). However, our previous and present measurements of D_{macro} for 16-PC in POPC agree with the FRAP results of Vaz et al. (5) within better than a factor of two even though the samples were prepared in totally different ways; furthermore our measurements of D_{micro} and D_{macro} were carried out on the same sample!

The discrepancy between D_{macro} and D_{micro} may reflect important details in the microscopic molecular dynamics. For example, D_{macro} involves motion of the whole labeled lipid over long distances, but at a molecular level we note that the ends of the long aliphatic chains enjoy much greater freedom of motion than the headgroups, which are constrained to lie within the surface plane of the bilayer. From Eq. 8 it is clear that our experiment measures dD_{micro}, and we have used the value of $d = 10$ Å corresponding to the rigid diameter of the lipid. However, a wagging of the chains would allow spin-exchange collisions to occur when radicals encounter at substantially longer distances. Thus, it may well be that one should use a significantly larger effective d in the analysis, and this would then yield a smaller D_{micro} than we have calculated. It would seem reasonable to account for a factor of no more than two by this mechanism. (Hyde and co-workers [39] have recently obtained results utilizing HE that would be consistent with such a model.) A second effect of the chain motion would be to reduce the number of encounters between labeled molecules on opposite sides of the bilayer, reducing the effective spin label concentration.

Another matter requiring detailed future consideration is the possible role of dimensionality, which has been discussed by Zientara and Freed (40) for HE and Korb et al. (41) for EED. In particular, these theoretical studies have shown the profound effects that more sophisticated analyses of two-dimensional motions in a plane have for both HE and EED. For example, for EED, the T_2^{-1} (EED) may be greatly enhanced beyond that of our simple modification given above (41). The microscopic *relative* diffusion that EED measures in two dimensions is also found to be extremely sensitive to the details of the membrane structure, and this suggests that our simple use of $U(r)$ and f^* in Eq. 5 will require significant modification as one develops more detailed models for EED and HE based on the dynamic structure of membranes. Clearly, the role of nonideal mixing on the dynamic structure can also be important. In the case of HE, the profound effect of dimensionality (even ignoring any role of dynamic structure) is closely related to that for the probability of first encounter of the exchanging radical pairs (40), originally discussed by Naqvi (42), which showed that for two dimensions, unlike three dimensions, it never even reaches a steady state. Finally, we note that effective dimensionality of the motion may differ from both the two-dimensional and three-dimensional models in biologically relevant cases of extreme membrane curvature. Although we regard such complex matters as beyond the scope of the present work, one may hope that future studies by spectral-spatial imaging could shed some light on these theoretical matters.

Another observation relates to the value of $U(d)$ of +1.6 kcal/mol obtained from the higher concentration range, which appears to imply a net repulsive interaction between colliding 16-PC molecules when they are in the milieu of other 16-PC molecules, but further studies are needed to confirm the accuracy of these details. We have refrained from detailed consideration of the lower concentration range spectra because of their lower signal-to-noise and inhomogeneous broadening. However, after correcting for the latter (cf. references 16 and 36) and considering possible distortions in our spectral-spatial imaging technique (U. Ewert and J. H. Freed, manuscript in preparation), we do find the $d\Delta H/dC$ slope anomalously large compared with that of the high concentration regime, but we feel further studies are needed to confirm this. At present, we cannot rule out the possibility of nonideal mixing in the POPC/16-PC model membrane leading to a nonlinear dependence of the line-broadening on concentration (26). (In fact, DSC experiments have indicated that POPC mixes nonideally with saturated acyl chain PCs such as DPPC [43].)

In conclusion, we have for the first time simultaneously measured both the D_{micro} for relative diffusion and the D_{macro} for self-diffusion of the same probe in the same model membrane sample. Consequently, an unambiguous comparison between D_{macro} and D_{micro} has been made which eliminates possible artifacts resulting from differences in probe molecules, sample preparation, hydration, etc., which are otherwise inevitable in comparisons of D_{micro} and D_{macro} measured by two different methods. We believe that such simultaneous measurements on various systems will provide an important tool to study the microscopic dynamic structure of membranes, and it will be extremely useful in the development of better models for molecular dynamics in membranes.

This work was supported by National Institutes of Health grant GM 25862 and National Science Foundation grants DMR89-01718 and CHE90-04552. Dr. Budil is a NIH National Research Service Award GM-12924 recipient.

Received for publication 31 July 1990 and in final form 7 November 1990.

REFERENCES

1. Gennis, R. B. 1989. Biomembranes, Molecular Structure and Function. Springer-Verlag, New York. 533 pp.
2. Kuo, A-L., and C. G. Wade. 1979. Lipid lateral diffusion by pulsed nuclear magnetic resonance. *Biochemistry.* 18:2300–2308.
3. Crawford, M. S., B. C. Gerstein, A.-L. Kuo, and C. G. Wade. 1980. Diffusion in rigid bilayer membranes. Use of combined multiple pulse and multiple pulse gradient techniques in nuclear magnetic resonance. *J. Am. Chem. Soc.* 102:3728–3732.
4. Rubenstein, J. L. R., B. A. Smith, and H. M. McConnell. 1979. Lateral diffusion in binary mixtures of cholesterol and phosphatidylcholines. *Proc. Natl. Acad. Sci. USA.* 76:15–18.
5. Vaz, W. L. C., R. M. Clegg, and D. Hallmann. 1985. Translational diffusion of lipids in liquid crystalline phase phosphatidylcholine multilayers. A comparison of experiment with theory. *Biochemistry.* 24:781–786.
6. Cleary, D. A., Y.-K. Shin, D. J. Schneider, and J. H. Freed. 1988. Rapid determination of translational diffusion coefficients using ESR imaging. *J. Magn. Reson.* 79:474–492.
7. Shin, Y.-K., and J. H. Freed. 1989. Dynamic imaging of lateral diffusion by electron spin resonance and study of rotational dynamics in model membranes. Effect of cholesterol. *Biophys. J.* 55:537–550.
8. Shin, Y.-K., J. K. Moscicki, and J. H. Freed. 1990. Dynamics of phosphatidylcholine-cholesterol mixed model membranes in the liquid crystalline state. *Biophys. J.* 57:445–459.
9. Moscicki, J. K., Y.-K. Shin, and J. H. Freed. 1991. EPR Imaging and in vivo EPR. G. Eaton, S. Eaton, and K. Ohno, editors. CRC Publishers, Boca Raton, FL. In press.
10. Mueller, H.-J., and H.-J. Galla. 1987. Chain length and pressure dependence of lipid translational diffusion. *Eur. Biophys. J.* 14:485–491.
11. Pfeiffer, W., G. Schlossbauer, W. Knoll, B. Farago, A. Steyer, and E. Sackmann. 1988. Ultracold neutron scattering study of local lipid mobility in bilayer membranes. *J. Phys. France.* 49:1077–1082.
12. Eastman, M. P., R. G. Kooser, M. R. Das, and J. H. Freed. 1969. Studies of Heisenberg spin exchange in ESR I. Linewidth and saturation effects. *J. Chem. Phys.* 51:2690–2709.
13. Trauble H., and E. Sackmann. 1972. Phase transition of lipid model membranes. III. Structure of a steroid-lecithin system below and above the lipid-phase transition. *J. Am. Chem. Soc.* 94:4499–4510.
14. Berner, B., and D. Kivelson. 1979. The electron spin resonance line width method for measuring diffusion. A critique. *J. Phys. Chem.* 83:1406–1412.
15. Popp, C. A., and J. S. Hyde. 1982. Electron-electron double resonance and saturation-recovery studies of nitroxide electron and nuclear spin-lattice relaxation times and Heisenberg exchange rates: Lateral diffusion in dimyristoyl phosphatidylcholine. *Proc. Natl. Acad. Sci. USA.* 79:2559–2563.
16. Sachse, J., D. M. King, and D. Marsh. 1987. ESR determination of lipid translational diffusion coefficients at low spin-label concentrations in biological membranes, using exchange broadening, exchange narrowing, and dipole-dipole interactions. *J. Magn. Reson.* 71:385–404.
17. Nayeem, A., S. B. Rananavare, V. S. S. Sastry, and J. H. Freed. 1989. Heisenberg spin exchange and molecular diffusion in liquid crystals. *J. Chem. Phys.* 91:6887–6905.
18. Ewert, U., and T. Herrling. 1986. Spectrally resolved EPR tomography with stationary gradient. *Chem. Phys. Lett.* 129:516–520.
19. Maltempo, M. M. 1986. Differentiation of spectral and spatial components in EPR imaging using 2-D image reconstruction algorithms. *J. Magn. Reson.* 69:156–161.
20. Maltempo, M. M., S. S. Eaton, and G. R. Eaton. 1987. Spectral-spatial two-dimensional EPR imaging. *J. Magn. Reson.* 72:449–455.
21. Maltempo, M. M., S. S. Eaton, and G. R. Eaton. 1988. Reconstruction of spectral-spatial two-dimensional EPR images from incomplete sets of projections without prior knowledge of the component spectra. *J. Magn. Reson.* 77:75–83.
22. Stemp, E. D. A., G. R. Eaton, S. S. Eaton, and M. M. Maltempo. 1987. Spectral-spatial electron paramagnetic resonance imaging and transport of radicals in nonuniform media. *J. Phys. Chem.* 91:6467–6469.
23. Woods, R. K., J. W. Dobrucki, J. F. Glockner, P. D. Morse II, and H. M. Swartz. 1989. Spectral-spatial ESR imaging as a method of noninvasive biological oximetry. *J. Magn. Reson.* 85:50–59.
24. Hornak, J. P., J. K. Moscicki, D. J. Schneider, and J. H. Freed. 1986. Diffusion coefficients in anisotropic fluids by ESR imaging of concentration profiles. *J. Chem. Phys.* 84:3387–3395.
25. Devaux, P., and H. M. McConnell. 1972. Lateral diffusion in spin-labeled phosphatidylcholine multilayers. *J. Am. Chem. Soc.* 94:4475–4481.
26. Eastman, M. P., G. V. Bruno, and J. H. Freed. 1970. ESR studies of Heisenberg spin exchange. II. Effects of radical charge and size. *J. Chem. Phys.* 52:2511–2522.
27. Ewert, U., T. Herrling, and W. Schneider. 1988. Advances in EPR tomography: methods and applications. *Exp. Techn. Physik (Jena, GDR).* 36:289–297.
28. Ewert, U., T. Herrling, and W. Schneider. 1989. EPR imaging. *Proc. 24th Ampere Congress, Posnan 1988, Poland.* J. Stankowski, N. Pislewski, S. K. Hoffmann and S. Idzink, editors. Elsevier, Amsterdam. 281–294. (A corrected version of this paper is available from the authors upon request.)
29. Lauterbur, P. C., D. N. Levin, and R. B. Marr. 1984. Theory and simulation of NMR spectroscopic imaging and field plotting by projection reconstruction involving an intrinsic frequency dimension. *J. Magn. Reson.* 59:536–541.
30. Bernardo, M. L., P. C. Lauterbur, and L. K. Hedges. 1985. Experimental example of NMR spectroscopic imaging by projection reconstruction involving an intrinsic frequency dimension. *J. Magn. Reson.* 61:168–174.
31. Deleted in proof.
32. Freed, J. H., and J. B. Pedersen. 1976. The theory of chemically induced dynamic spin polarization. *Adv. Magn. Reson.* 8:1–84.
33. Freed, J. H. 1977. Chemically Induced Magnetic Polarization. L. T. Muus, P. W. Atkins, K. A. McLauchlan, and J. B. Pedersen, editors. Reidel, Dordrecht, the Netherlands. 309–355.
34. Hwang, L. P., and J. H. Freed. 1975. Dynamic effects of pair correlation functions on spin relaxation by translational diffusion in liquids. *J. Chem. Phys.* 63:4017–4025.
35. Lis, L. J., M. McAlister, N. Fuller, R. P. Rand, and V. A. Parsegian. 1982. Interactions between neutral phospholipid bilayer membranes. *Biophys. J.* 37:657–665.
36. Lang, J. H., and J. H. Freed. 1972. ESR study of Heisenberg spin exchange in a binary liquid solution near the critical point. *J. Chem. Phys.* 56:4103–4114.
37. Bales, B. L., J. A. Swenson, and R. N. Schwartz. 1974. Electron

paramagnetic resonance studies of Heisenberg spin exchange in a nematic liquid crystal. *Mol. Cryst. Liq. Cryst.* 28:143–153.

38. Saxton, M. J. 1989. Lateral diffusion in an archipelago. Distance dependence of the diffusion coefficient. *Biophys. J.* 56:615–622.
39. Yin, J.-J., J. B. Feix, and J. S. Hyde. 1990. Mapping of collision frequencies for stearic acid spin labels by saturation-recovery electron paramagnetic resonance. *Biophys. J.* 58:713–720.
40. Zientara, G. P., and J. H. Freed. 1979. Chemically induced dynamic spin polarization in two dimensional system: theoretical predictions. *J. Chem. Phys.* 71:3861–3879.
41. Korb, J.-P., M. Ahadi, G. P. Zientara, and J. H. Freed. 1987. Dynamic effects of pair correlation functions on spin relaxation by translational diffusion in two-dimensional fluids. *J. Chem. Phys.* 86:1125–1130.
42. Naqvi, R. 1974. Diffusion-controlled reactions in two-dimensional fluids: discussion of measurements of lateral diffusion of lipids in biological membranes. *Chem. Phys. Lett.* 28:280–284.
43. Curatolo, W., B. Sears, and L. J. Neuringer. 1985. A calorimetry and deuterium NMR study of mixed model membranes of 1-palmitoyl-2-oleoyl-phosphatidylcholine and saturated phosphatidylcholines. *Biochim. Biophys. Acta.* 817:261–270.